Acta Oceanol. Sin., 2015, Vol. 34, No. 6, P. 101–112
DOI: 10.1007/s13131-015-0690-z
http://www.hyxb.org.cn
E-mail: hyxbe@263.net

Satellite remote sensing of ultraviolet irradiance on the ocean surface

LI Teng[1], PAN Delu[1, 4], BAI Yan[1, 4]*, LI Gang[2], HE Xianqiang[1], CHEN Chen-Tung Arthur[3], GAO Kunshan[5], LIU Dong[1], LEI Hui[4]

[1] State Key Laboratory of Satellite Ocean Environment Dynamics, Second Institute of Oceanography, State Oceanic Administration, Hangzhou 310012, China

[2] Key Laboratory of Tropical Marine Bio-resources and Ecology, South China Sea Institute of Oceanology, Chinese Academy of Sciences, Guangzhou 510301, China

[3] Institute of Marine Geology and Chemistry, College of Marine Sciences, National Sun Yat-Sen University, Kaohsiung 80424, Taiwan, China

[4] Institute of Remote Sensing and Earth Science, Hangzhou Normal University, Hangzhou 311121, China

[5] State Key Laboratory of Marine Environmental Science, Xiamen University, Xiamen 361005, China

Received 26 January 2014; accepted 7 August 2014

Abstract

Ultraviolet (UV) radiation has a significant influence on marine biological processes and primary productivity; however, the existing ocean color satellite sensors seldom contain UV bands. A look-up table of wavelength-integrated UV irradiance (280–400 nm) on the sea surface is established using the coupled ocean atmosphere radiative transfer (COART) model. On the basis of the look-up table, the distributions of the UV irradiance at middle and low latitudes are inversed by using the satellite-derived atmospheric products from the Aqua satellite, including aerosol optical thickness at 550 nm, ozone content, liquid water path, and the total precipitable water. The validation results show that the mean relative difference of the 10 d rolling averaged UV irradiance between the satellite retrieval and field observations is 8.20% at the time of satellite passing and 13.95% for the daily dose of UV. The monthly-averaged UV irradiance and daily dose of UV retrieved by satellite data show a good correlation with the *in situ* data, with mean relative differences of 6.87% and 8.43%, respectively. The sensitivity analysis of satellite inputs is conducted. The liquid water path representing the condition of cloud has the highest effect on the retrieval of the UV irradiance, while ozone and aerosol have relatively lesser effect. The influence of the total precipitable water is not significant. On the basis of the satellite-derived UV irradiance on the sea surface, a preliminary simple estimation of ultraviolet radiation's effects on the global marine primary productivity is presented, and the results reveal that ultraviolet radiation has a non-negligible effect on the estimation of the marine primary productivity.

Key words: ultraviolet radiation, remote sensing, radiative transfer, marine primary productivity

Citation: Li Teng, Pan Delu, Bai Yan, Li Gang, He Xianqiang, Chen Chen-Tung Arthur, Gao Kunshan, Liu Dong, Lei Hui. 2015. Satellite remote sensing of ultraviolet irradiance on the ocean surface. Acta Oceanologica Sinica, 34(6): 101–112, doi: 10.1007/s13131-015-0690-z

1 Introduction

The ultraviolet radiation (UVR), with wavelengths between 10 and 400 nm, is an important component of solar radiation (Hou et al., 2012). Owing to the selective absorption of the UVR by ozone, only the longer wavelength UVR (>280 nm) can travel to the earth's surface. In studies, the UVR was divided into wavelength-integrated UVA (315–400 nm) and UVB (280–315 nm) (Jin et al., 2009). Although the intensity of the UVR on the ground accounts for only 0.71%–0.86% (UVB) and 15.5%–17.8% (UVA) of the visible radiation (≈400–700 nm) on the ocean surface (Gao et al., 2007a), the photon energy of the UVR is much higher, causing severe damage to phytoplankton. The UVR has been reported to affect aquatic ecosystems and the carbon cycle. For example, the high-intensity UVR can damage the photosynthetic pigments of phytoplankton cells (Pang et al., 2010), inhibit the photosynthetic ability of phytoplankton (Li et al., 2011), induce cell mortality (Agustí and Llabrés, 2007), and reduce the marine primary productivity (MPP) (Häder, 2011), etc. The inhibitory effect of the UVR on the carbon fixation of the surface phytoplankton can be up to 29% in the South China Sea (Li et al., 2011). On the other hand, the UVA can enhance the productivity of phytoplankton under low solar irradiance or strong vertical mixing conditions where microplankton is dominant (Nilawati et al., 1997; Barbieri et al., 2002; Li and Gao, 2013). Experiments around Nan'ao Island show that the MPP in the tropical coastal sea can be increased by about 13% induced by the UVR (Gao et al., 2007b). However, most of the existing satellite remote sensing models of the MPP only take account of the photosynthetically active radiation (PAR) (the wavelength-integrated solar visible radiation from 400 to 700 nm), and the effects of the UVR are ignored.

Foundation item: The Public Science and Technology Research Funds Projects for Ocean Research of China under contract No. 201505003; the National Basic Research Program (973 Program) of China under contract No. 2015CB954002; the National Natural Science Foundation of China under contract Nos 41476155, 41322039, 41271378 and 41206168.

*Corresponding author, E-mail: baiyan@sio.org.cn

The data from ocean color satellite sensors, e.g., the moderate resolution imaging spectroradiometer (MODIS) and the sea-viewing wide field-of-view sensor (SeaWiFS), currently used for estimating MPP provide no information in the ultraviolet (UV) bands, with 412 nm being the shortest wavelength detected. However, as a sensor used for atmospheric studies, the ozone monitoring instrument (OMI) on board the "Aura" satellite can provide UV irradiance products, but it can only observe at the satellite's passing time (about 13:45 local time) and specific wavelengths (305, 310, 324 and 380 nm). In addition, the total ozone mapping spectrometer (TOMS) on board the "Nimbus-7" can measure the erythemal UV irradiance (the potential for biological damage due to the solar radiation, which can be calculated by using the UV irradiance reaching the surface of the earth and weighted by model values of susceptibility of Caucasian skin to sunburn (erythema)). Therefore, there is still no satellite that provides information about daily dose of UV (the diurnally integrated amount of the UV radiation), especially the wavelength-integrated daily dose of UV at 280–400 nm, which is needed in the study of the MPP (Tanskanen et al., 2006; Torres et al., 2007). To quantitatively evaluate the effects of the UVR on the MPP on a global scale, the global distribution of the UVR on the sea surface needs to be retrieved using satellite remote sensing data.

The atmospheric radiative transfer models have also been used to estimate the UV irradiance arriving at the sea surface using the known composition of the atmosphere (Herman et al., 1999; Vasilkov et al., 2001; Ahmad et al., 2003; Smyth, 2011). On the basis of the radiative transfer model, the global distribution of monthly integrated UV-erythemal irradiance (290–400 nm) on the earth's surface was estimated, by including total ozone amount, cloud transmittance, aerosol amount, surface reflectivity of the solar UV radiation backscattered from the earth's atmosphere, and the extraterrestrial solar irradiance in the calculation (Herman et al., 1999), but such a calculation is quite complicated and inefficient. To improve the computational efficiency, Ahmad et al. (2003) established a look-up table of the surface UVR intensity based on the ozone concentration, the cloud reflectivity, the aerosol optical thickness, and the solar zenith angle, and calculated the surface UV irradiance at the local noontime. Smyth (2011) retrieved the sea-surface UV irradiance at noon through a look-up table, and estimated the daily dose of UV at separate wavelengths (305, 325, 340 and 380 nm) by assuming that the intensity of UVR during the day changes following a sinusoidal function. However, the diurnal variation of the UV irradiance under the influence of weather/cloud variation also has a great effect on the photosynthesis of phytoplankton.

With the aim to future analysis of the UVR's effect on MPP estimation, we develop a method to retrieve the wavelength-integrated UV irradiance (280–400 nm) on the sea surface by using satellite atmospheric data. First, a look-up table of the wavelength-integrated UV irradiance was established using the coupled ocean atmosphere radiative transfer (COART) model. It was then used to retrieve the global distribution of the sea-surface UV irradiance using the solar zenith angle, the aerosol optical thickness at 550 nm, the ozone amount, the liquid water path, and the total precipitable water at middle and low latitudes. All of these inputs used in the inversion can be obtained by satellite remote sensing. Second, the satellite-retrieved UV irradiance was validated using the *in situ* data and finally the sensitivity of the UV irradiance on the different components of the atmosphere was analyzed.

2 Data

2.1 *In situ sea-surface UV irradiance data*

Two *in situ* data sets were used in this study (Fig. 1). The *in situ* data of 2006 were obtained from the World Ozone and Ultraviolet Radiation Data Center (WOUDC, red stations in Fig. 1). Most observing data from the WOUDC stations did not contain the complete wavelength from 280 to 400 nm. In all of the nearshore WOUDC stations, there are only two stations which measure the UV irradiance from 280 to 400 nm; one is the San Diego Station (32°45′58″N, 117°11′42″W) on the west coast of the USA, and the other is the Ushuaia Station (54°49′19″S, 68°19′23″W) in Argentina. The instrument used at these two sites is a surface biospherical UV scanner (SUV-100), working in the spectral mode, with 2 nm intervals from 280 to 400 nm. The frequency of measurement was about 15 min. In this study, we used the integrated irradiance from 280 to 400 nm.

The *in situ* data of 2011 are obtained from the station (24°N, 118°E) at Xiamen University in China, with an Eldonet broad band filter radiometer (blue station in Fig. 1). This equipment has

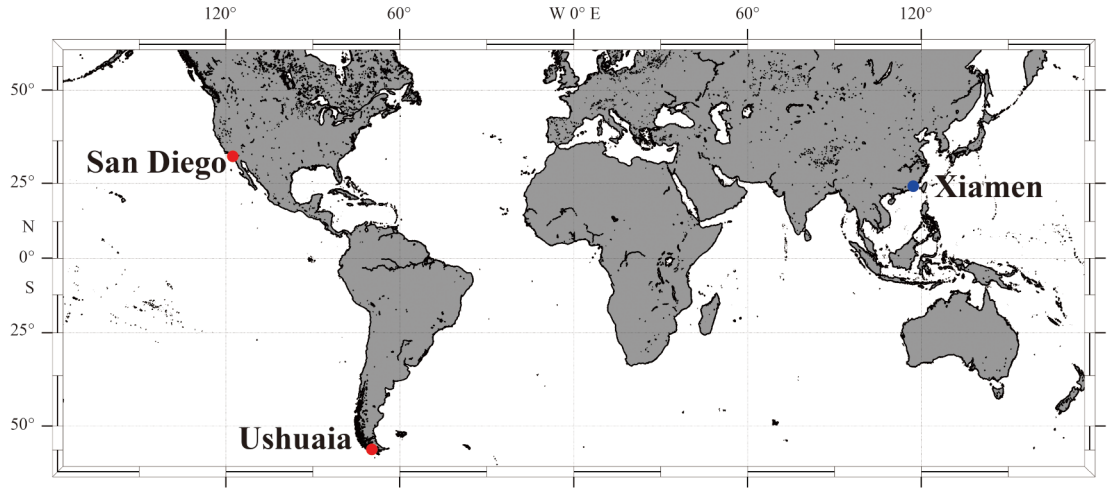

Fig. 1. Locations of *in situ* data stations.

three channels: PAR (400–700 nm), UVA (315–400 nm), and UVB (280–315 nm) irradiance and measures the light levels every second but records the means over each minute.

2.2 *Satellite data*

Satellite products used in this paper were mainly from the MODIS and the atmospheric infrared sounder (AIRS), which are both on board the "Aqua" satellite. The aerosol optical thickness and liquid water path products were from the MODIS, while the ozone amount and the total precipitable water were from the AIRS. Details of the satellite products can be seen in Table 1. Among them, the products with lower spatial resolution (1°× 1°) were used to retrieve the ocean surface UV irradiance, while the product with a resolution of 1 km×1 km was used in the validation of satellite-derived surface UV irradiance.

The monthly-averaged surface PAR from the MODIS was also gathered to make a comparison with the distribution of the surface UVR. The spatial resolution of satellite-derived PAR is 9 km×9 km. For the direct comparison between the PAR and the UVR, the satellite-derived PAR (Einstein/(m^2·d^{-1})) needs to be converted to the same unit (W/m^2) of the UVR as Eq. (1) (Frouin and Pinker, 1995):

$$PAR = \frac{D_{\mathrm{irr}}}{khc}\int_{0.4}^{0.7}\lambda I(\lambda)\mathrm{d}\lambda, \tag{1}$$

where D_{irr} is the photoperiod (s), which is determined by the solar zenith angle at a certain location and date; k is the Avogadro constant (≈6.022×10^{23}); h is Planck's constant (6.63×10^{-34} J·s); c is the speed of light in a vacuum (3×10^8 m/s) and $I(\lambda)$ is the PAR irradiance (W/m^2). Because the PAR from the satellite is wavelength integrated, λ is set as the middle wavelength (550 nm) of the PAR.

All the satellite products were downloaded from the following NASA website (http://oceancolor.gsfc.nasa.gov).

Table 1. Details of satellite products

	Total precipitable water/kg·m^{-2}	Ozone amount/Dobson	Aerosol optical thickness (550 nm)/dimensionless	Liquid water path/g·m^{-2}
Data source	Aqua/ARIS	Aqua/ARIS	Aqua/MODIS	Aqua/MODIS
Spatial resolution	1°×1°	1°×1°	1°×1°	Level 3: 1°×1° Level 2: 1 km×1 km
Products level	Level 3: daily and monthly	Level 3: daily and monthly	Level 3: daily and monthly	Level 3: daily and monthly Level 2: daily

3 Retrieval method for sea-surface UV irradiance

3.1 *Generating the look-up table by the radiative transfer model*

The absorption, scattering, and transmittance of the solar irradiance through the atmosphere can be calculated by the radiative transfer model. In this paper, the COART model developed by Jin and Stamnes (1994) was used in the establishment of the sea-surface UV irradiance look-up table. The COART simulates the absorption and scattering caused by atmospheric molecules, aerosols, ozone, clouds, as well as particles and dissolved substances in water, which can be used to calculate the irradiance and radiance at any level of the atmosphere and ocean in both narrow band (spectrum) and broad band (integrated wavelength) between 200 and 100 000 nm (Jin et al., 2006).

Ozone can absorb the UV radiation strongly, especially UVB (Wang et al., 1999); the intensity of the UVB on the ground is less than 1% that of the total solar radiation on the top of the atmosphere (Pang et al., 2010). The attenuation of the UVA on the other hand is mainly caused by the scattering of atmospheric molecules, aerosols, and clouds (Guo et al., 2002). Therefore, we chose the input parameters for the atmospheric conditions for the generation of the sea-surface UV irradiance look-up table to be the ozone amount, the aerosol optical thickness at 550 nm, the liquid water path, and the total precipitable water. In this study, our target area is between 60°N and 60°S. The types of atmosphere are set as tropical, middle latitude summer, and middle latitude winter. The aerosol type in the troposphere is set as the maritime aerosol. Compared with the large variation of aerosols in the troposphere, the aerosols in the stratosphere are relatively stable. Therefore, the type of stratospheric aerosol is set as background in the COART model, and cloud is set as isotropic. In addition, because the effects of ocean surface roughness on the downward radiation in the atmosphere are negligible (Jin et al., 2006), a flat surface is adopted in the COART model, and the radiation is considered completely absorbed by the sea water.

Table 2 shows the details of the input parameters for the generation of the look-up table. The outputs are the wavelength-integrated irradiance of the UVA and the UVB.

Table 2. Input parameters in COART model for the generation of the UVR look-up table

Parameters	Range	Step
Solar zenith angle/(°)	0–85	5
Ozone amount/atm-cm	0.10–0.50	0.05
Aerosol optical thickness (550 nm)	0.0–0.5, 0.6, 0.7	0.05
Total precipitable water/g·cm^{-2}	0–6	1
Liquid water path/g·m^{-2}	0–350	50

3.2 *Retrieval method using satellite data*

To calculate the surface UV irradiance, the solar zenith angle of each satellite pixel and the type of atmosphere are calculated, firstly, on the basis of geographical position and observing time of satellite. In the Northern Hemisphere, the summer atmosphere is considered to last from April to September, with the rest of the year considered to be the winter atmosphere; note that seasonal setting for the Southern Hemisphere is the opposite of that for the Northern Hemisphere. Therefore, maps of the surface UV irradiance are obtained by inputting the satellite products of the aerosol optical thickness (550 nm), the ozone amount, the liquid water path, and the total precipitable water from the same day along with the solar zenith angle into the look-up table. In the inversion, any invalid inputted data from the

daily atmospheric products are replaced by monthly-averaged data for the same pixel.

Note that the unit of ozone amount inputted into the look-up table is atm-cm; however, the unit of the satellite-derived ozone amount is Dobson. Unit conversion is needed before using the satellite product of the ozone amount, by using Eq. (2):

$$1\ \text{atm-cm} = 1\,000\ \text{Dobson}. \tag{2}$$

In the inversion of the daily UVR dose, atmospheric conditions are assumed to be constant during the day. Atmospheric products at the satellite's passing time are inputted into the look-up table, while the solar zenith angle is calculated for each pixel every half an hour from sunrise to sunset. The UV irradiance is inversed at each solar zenith angle so as to describe the diurnal variation of the sea-surface UVR. Then, the daily dose of UV at each pixel is calculated by integrating the discrete UV irradiance in the day length.

3.3 *Satellite results*

With the generated look-up table and the satellite-derived atmospheric products, the monthly-averaged UV irradiance and the PAR irradiance on the ocean surface were produced, and here we use the data from 2006 as an example (Fig. 2). Globally, the surface UV irradiance and the PAR irradiance range from 0 to 40 W/m^2 and from 0 to 300 W/m^2, respectively. The averaged surface UV irradiance accounts for about 10% of the averaged surface PAR irradiance. Compared with the distribution of the PAR on the sea surface, the geographical distribution of the UVR is more variable because it is more sensitive to the attenuation of the atmosphere.

Temporally, the distributions of the surface UV and PAR irradiance have a significant seasonal variation correlated closely with the solar zenith angle, which is a major factor in controlling the seasonal solar distribution. The transmission path of the solar radiation in the atmosphere becomes longer with an increase in the solar zenith angle (July for the Northern Hemisphere and January for the Southern Hemisphere), and the attenuation of the solar radiation caused by ozone, water vapor, clouds, and aerosols increases, resulting in small surface UV and PAR irradiance.

Geographically, both the spatial variations of the UV irradiance and the PAR are related to the spatial distribution of the atmospheric composition. In the tropical ocean, the UV and the PAR irradiance are high over the entire year. However, the regions with the highest UV and PAR irradiance are located in the subtropics, where the frequency of clear days is high.

Globally, the geographical distribution of the PAR is more continuous. The areas with the highest PAR irradiance are mainly in the open ocean (the middle of the Pacific, the Atlantic, the Arabian Sea and the Indian Ocean) and the annual averaged PAR irradiance is higher in the Southern Hemisphere. Compared with the PAR, the geographical distribution of the UVR is relatively scattered, the regions with the highest surface UV irradiance in the Northern Hemisphere summer (July) are the Arabian Sea, the South China Sea, and the western coastal oceans of America and Africa. For the corresponding conditions during the Southern Hemisphere summer (January), the regions with the highest UV and PAR irradiance are the western seas of Africa, South America, and Australia and the eastern sea of Africa. These regions are located in the subtropics, where the frequency of clear days is high. In addition, because there are more clear days in April than in October, the UV irradiance in April in the tropical ocean is relatively higher, which is consistent with the analysis of previous research (Herman et al., 1999).

4 Validation and discussion

4.1 *Validation of satellite-derived ultraviolet irradiance*

For accurate comparison, the satellite-retrieved UV irradiance and the *in situ* data must be matched in both time and space. Here, the matching criteria are that (1) the time interval between the satellite observation and the *in situ* measurement should be less than 7.5 and 2.0 min according to the field-measure frequency, respectively, and (2) the distance between the satellite image pixel and the *in situ* station should be less than 10 km.

It should be noted that although the field measurements are continuous during the day, the measured frequency is about 15 and 1 min for the data in 2006 and 2011, respectively. Therefore, the observation time between the *in situ* data and the satellite data cannot match exactly. On the other hand, compared with the *in situ* data measured at one spot, the satellite data are area-averaged values determined by the spatial resolution of the satellite products. To improve the spatial resolution, we use Level 2 products of the liquid water path (representing the cloud condition) with higher spatial resolution (1 km×1 km) in the validation. In addition, because the spatial variations of the aerosol optical thickness, the ozone amount and the total precipitable water are relatively low, Level 3 products of these parameters (1°×1°) were used in the validation.

The validation results at San Diego (USA), Ushuaia (Argentina), and Xiamen University (China) are shown in Fig. 3. The temporal variation of the satellite-derived UV irradiance and the *in situ* measurement are consistent over the whole year. Overall, the inversed UV irradiance and *in situ* values are consistent, with a standard deviation① and mean relative difference② of 10 W/m^2 and 24.74%, respectively, at San Diego (Figs 3a and b), and 14.92 W/m^2 and 20.74%, respectively, at Xiamen University (Fig. 3e and f). The satellite-derived UV irradiance is, overall, less than that of the *in situ* observation at Ushuaia, with standard deviation and mean relative difference of 11 W/m^2 and 38.06%, respectively (Figs 3c and d). Some of the large deviation may result from the temporal and spatial mismatch between satellite and *in situ* observations. Although we have restricted the distance between the ground station and satellite data to be 10 km, the ground meas-

① The calculation of the standard deviation is $d_s = \sqrt{[1/(n-1)]\sum_{i=0}^{n}(E_{rs}-E_{is})^2}$, where E_{rs} and E_{is} are UV irradiance of satellite inversion and ground measurement, respectively; n is the number of calculations.

② The calculation of the mean relative difference is $d_m = \sum_{i=1}^{n}|(E_{rs}-E_{is})/E_{is}|$, where E_{rs} and E_{is} are UV irradiance of satellite inversion and ground measurement, respectively; n is the number of calculations.

urement usually corresponds to a much smaller area. The mismatch in space would induce errors in the comparison, especially when fractus clouds exist. On the other hand, when the weather is changing quickly, the mismatch in time can also lead to large deviation in the comparison.

Since the mismatch is random, time-averaged or time-integrated quantitative analysis may reduce the uncertainties (Herman et al., 1999; Wang et al., 2001). Figure 4 shows the comparisons of the surface UV irradiance of a rolling average of 10 and 30 d. The satellite estimations closely follow the fluctuation of the ground measurement at San Diego and Xiamen University. However, the satellite results at Ushuaia are obviously less than the ground observations. Comparing with the rolling average of 10 d for the ground observations, the standard deviation and mean relative difference of satellite results are 4.16 W/m^2 and 8.23% for San Diego, 8.3 W/m^2 and 35.46% for Ushuaia, and 7.05 W/m^2 and 10.54% for Xiamen University, respectively. For the data with a rolling average of 30 d, a good linear relationship was found between the satellite results and the ground observations with an *r*-square value of 0.95, 0.83 (Fig. 4d) and 0.96, standard deviations of 2.75, 8.11 and 5.49 W/m^2, and mean relative differences of 6.57%, 40.24% and 9.66%, for San Diego, Ushuaia, and Xiamen University, respectively. The large difference at Ushuaia might be caused by applying the middle latitude atmosphere to the high latitude region of Ushuaia. In fact, the attenuation of the UVR in the middle latitude atmosphere is higher than that in the high latitude atmosphere. Thus, using the middle latitude atmosphere in the inversion of the UV irradiance at Ushuaia may result in a systematic underestimation of the satellite-derived UV irradiance.

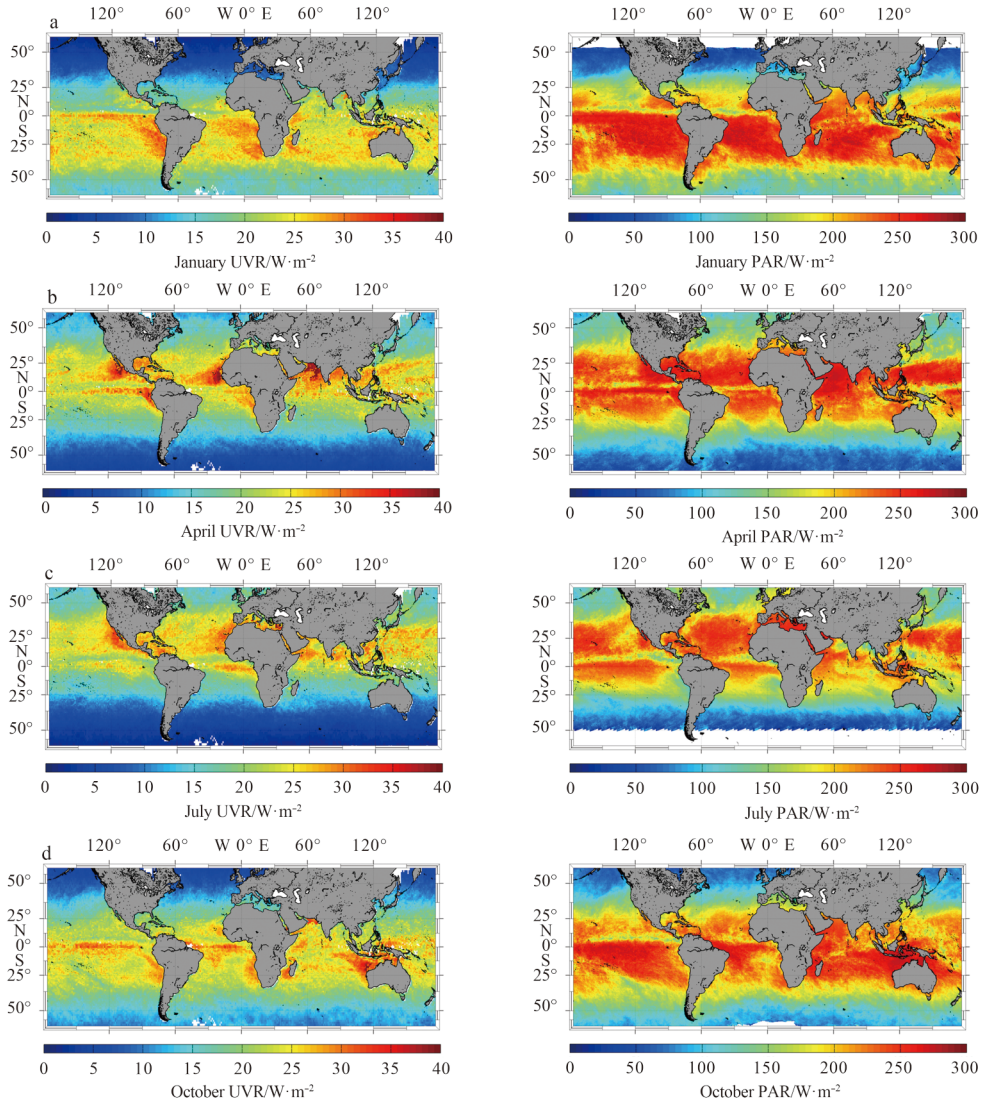

Fig. 2. The distribution of the inversed monthly-averaged UV irradiance (left hand side) and PAR irradiance (right hand side) on the ocean surface in 2006. Figs 2a, b, c, and d show the results of January, April, July, and October, respectively.

4.2 *Sensitivity analysis*

In order to understand the influence of the accuracies of different inputted atmospheric parameters on the retrieved UVR, we conducted a sensitivity analysis. The atmosphere type was set as mid-latitude summer. First, the standard UV irradiance was retrieved by using the annual mean values of the solar zenith angle, the total precipitable water (TOW), the ozone amount (OA), the aerosol optical thickness (550 nm) (AOT), and the liquid water path (LWP), at San Diego (Table 3). Then, we changed one of the inputted parameters each time with a step of 20% and

variation ranging from +80% to –80%.

Thus, the sensitivity (s) is calculated as follows:

$$s = \left(\frac{E_{uvr1} - E_{uvr2}}{E_{uvr2}} \right) \times 100\%, \quad (3)$$

where E_{uvr1} is the changed retrieved UVR after changing one specific inputted parameter; E_{uvr2} is the standard UV irradiance with the annual mean values.

The sensitivities of the retrieved UV irradiance to all inputted parameters are shown in Fig. 5. The most sensitive parameters are the solar zenith angle and the liquid water path. With the increase of the solar zenith angle, the transmission path of radiation in the atmosphere becomes longer and results in more attenuation of the UVR. The liquid water path representing the cloud condition can strongly absorb the UVR, and have a significant influence on the UV irradiation. The sensitivities of the retrieved UV irradiance resulting from the variations of the ozone, the aerosol optical thickness (550 nm), and the total precipitable water are much smaller (Fig. 5a). To further check the effects of these three parameters, we calculate the sensitivities of the UV irradiance with a liquid water path of 0 g/m² and a solar zenith angle of 30° (Fig. 5b). The sensitivities range from –1.75% to 3% for the ozone, –1.75% to 2% for the aerosol optical thickness (550 nm), and less than 0.5% for the total precipitable water. Overall, the high-varying cloud condition (the liquid water path) has remarkable influence on the retrieval of the UV irradiance, and it needs higher spatial and temporal remote sensing observations.

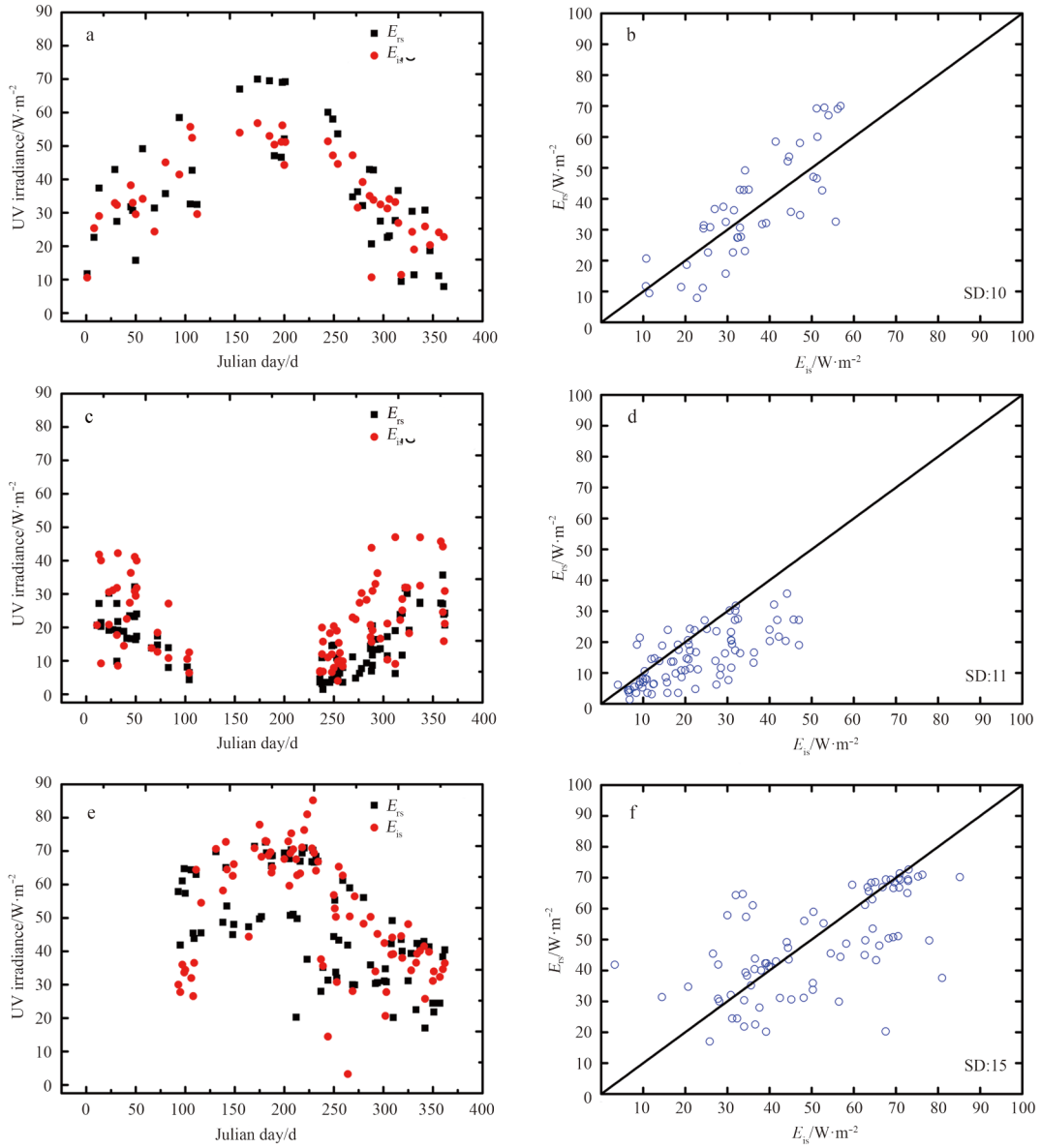

Fig. 3. The annual variation of satellite-derived (remote sensing) UV irradiance (E_{rs}) and *in situ* UV irradiance (E_{is}) for San Diego, USA (a and b); Ushuaia, Argentina (c and d) and Xiamen University in China (e and f). Note that the latitude of Ushuaia is high (54°49′19″S), and data are missing during the Southern Hemisphere winter because of the polar night (Julian days 105–235 d, Fig. 3c).

Table 3. Annual mean values of inputted parameters

Zenith angle/(°)	TOW/kg·m^{-2}	OA/Dobson	AOT (550 nm)	LWP/g·m^{-2}
45	1.807 0	0.300 5	0.111 4	68.916 7

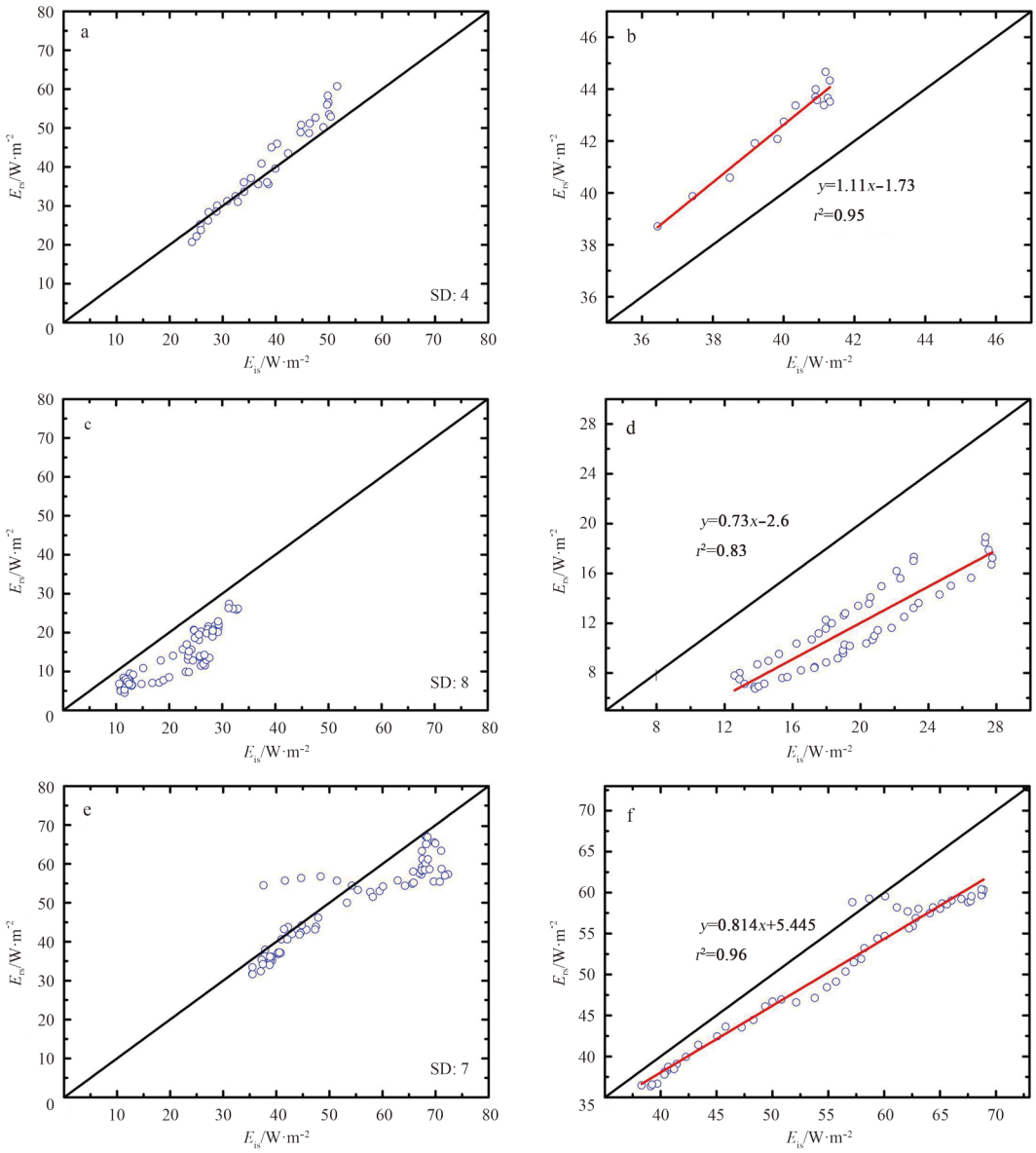

Fig. 4. Comparisons of 10 d (a, c and e) and 30 d (b, d and f) rolling averaged surface UV irradiance for San Diego, USA (a and b); Ushuaia, Argentina (c and d) and Xiamen University in China (e and f). E_{rs} and E_{is} are satellite-derived data and *in situ* data, respectively; SD is standard deviation; the black lines are 1:1 lines, and the red lines are linear regression lines.

4.3 *Diurnal variation*

The diurnal variation of the UV irradiance on the sea surface has a great effect on the estimate of the marine primary production. However, a satellite can only provide local atmospheric products at its passing time, and the sensitivity analysis has shown that the variation of input parameters, especially the variation of the liquid water path, has a great effect on the retrieved UV irradiance. As in the comparison in Fig. 3, we chose 3 d at each ground station with relatively small and high relative differences of satellite-derived results to check the UV irradiance diurnal variation and the effects of the atmosphere on the validation (Fig. 6).

At San Diego, the relative differences between the satellite-derived UV irradiance and the *in situ* data are 7.0%, 93.0% and 65.0% on Julian days 47, 288, and 361, respectively; at Ushuaia, the relative differences on Julian days 15, 32, and 360 are 132.0%, 124.0% and 10.0%, respectively; at Xiamen University, the relative differences on Julian days 234, 244, 264 are 1.4%, 116.6%, and 1 186.4%, respectively. Obviously, the higher diurnal variation of the surface UV irradiance corresponds to a larger relative difference between the satellite-derived UV irradiance and the *in situ* data, and vice versa, indicating that the diurnal variations have a remarkable effect on the validation of the satellite-derived UV irradiance.

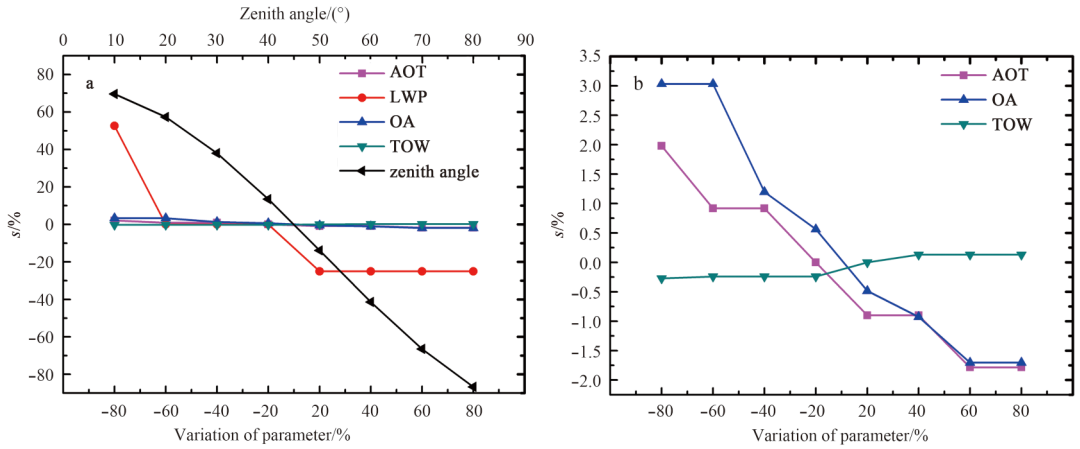

Fig. 5. The sensitivities of retrieved UV irradiance (*s*) to five inputted parameters (the variation of LWP, OA, TOW, and AOT ranges between +80% and –80% with a step of 20%; the variation of the zenith angle ranges from 0° to 90° with a step of 10°) (a) and the sensitivity to AOT, OA, and TOW with an LWP of 0 g/m² and zenith of 30° in 2006 at San Diego, USA (b).

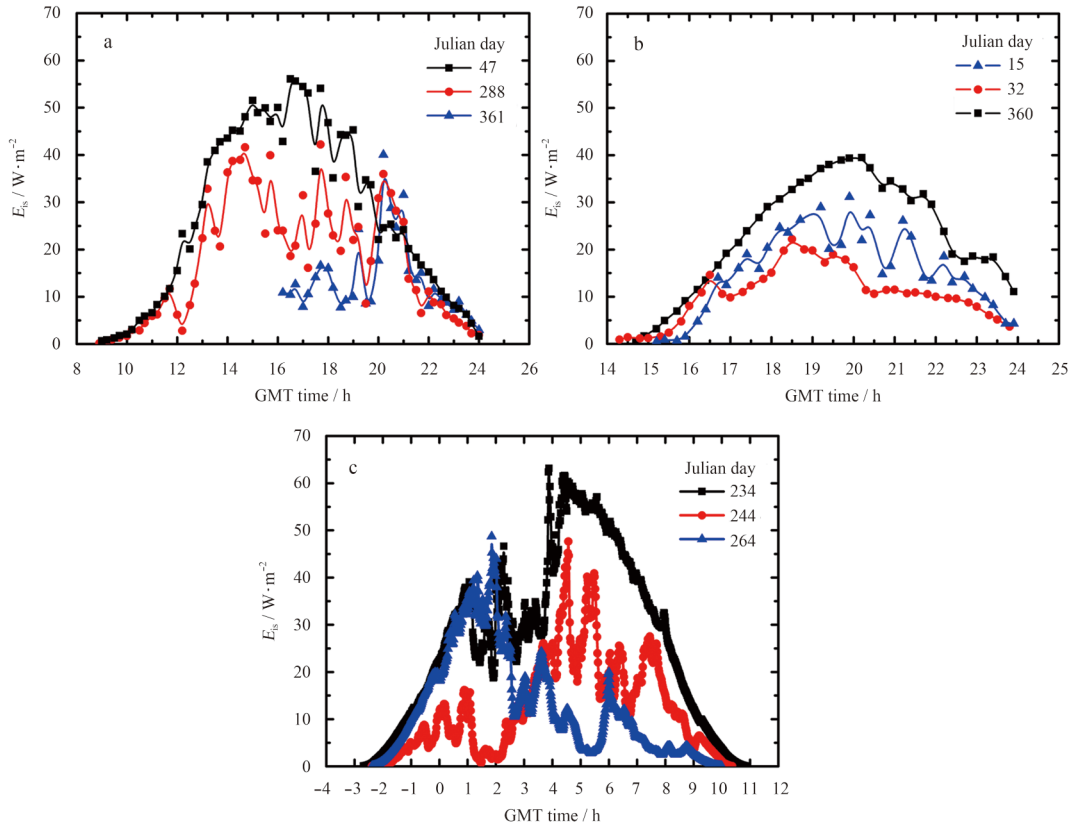

Fig. 6. The diurnal variations of the *in situ* UV irradiance at San Diego, USA (a), Ushuaia, Argentina (b) and Xiamen University (c).

To quantitatively examine the diurnal variation of atmospheric conditions on the estimation of the diurnal UV irradiance, the liquid water path and the aerosol optical thickness (550 nm) from the satellites "Terra" (passing time approximately 10:30) and "Aqua" (passing time approximately 13:30) are used for comparison (Fig. 7). The diurnal variation of the ozone amount and the total precipitable water are ignored. During the hours of sunshine (the time of day length), individual "Terra" and "Aqua" data are used before 10:30 and after 13:30, respectively; a linear interpolation is used for data between 10:30 and 13:30. Figure 7 shows the comparison of the daily dose of UV between the ground observations and the satellite estimations at San Diego. The standard deviations are 0.37 MJ/(m²·d) when using the data from the two satellites (Fig. 7a), and 0.40 MJ/(m²·d) when using only the "Aqua" data (Fig. 7b), with mean relative differences of 27.01% and 28.66%, respectively. On the 30 d rolling average scale, the standard deviations are 0.10 MJ/(m²·d) when using the data from the two satellites, and 0.12 MJ/(m²·d) when using only the "Aqua" data, with mean relative differences of 6.71% and 8.43%, respectively. Compared with the results when using only the "Aqua" data, the validation results are better, and the mean relative difference decreases 20.40% on the 30 d average scale by using data from two satellites.

Figure 8 shows the annual variation of the daily dose of UV.

The retrieved results using different satellite data show similar trends and good agreement with the field data in winter and early spring. During the summer months, the fluctuation of the retrieved results around the *in situ* observation increases due to the high frequency of cloudy days. Therefore, satellite products with a higher temporal resolution are needed to improve the inversion accuracy of the daily dose of surface UV.

5 Concluding remarks

A satellite retrieval method of the wavelength-integrated UV irradiance at middle and low latitudes ocean surface was established in this study. For fast calculation, a look-up table was generated using the radiative transfer model. All the inputted atmospheric parameters in the look-up table can be obtained from satellite products. On the basis of the generated look-up table, the maps of the ocean surface UV irradiance were derived using the atmospheric data from the "Aqua" satellite.

The time series of ground-based measurements of the surface UV irradiance from the WOUDC in 2006 and from the data measured at Xiamen University in 2011 were used to validate the accuracy of the satellite-derived results. On a 10 d rolling average scale, the mean relative differences of the retrieved UV irradiance and the daily dose were 8.22% and 13.95%, respectively. On a 30 d rolling average scale, the mean relative differences of the retrieved UV irradiance and the daily dose were 6.57% and 8.43%, respectively. The temporal variation between the satellite retrievals and ground observations is consistent over the whole year. The cloud (represented by the liquid water path) is the most sensitive parameter affecting the accuracy of the ocean surface UV irradiance inversion. Since the existing satellite with the surface UV irradiance monitoring ability is mainly focused on the atmosphere, special ocean color sensors for monitoring the surface UV irradiance with high signal to noise ratio and temporal resolution will be helpful in research on the UVR's effects on marine ecosystems and MPP.

Currently, Cullen et al. (2012) estimated a spectral depth-integrated photosynthesis model with five biological weighting functions for the inhibition of UVR and assess the global MPP by using satellite retrieved chlorophyll. However, the most existing satellite remote sensing of the marine primary production only considers the effects of visible light radiation, ignoring the UVR. With the availability of the satellite-derived UV irradiance, we make a preliminary simple analysis of the effects of the UVR on the primary productivity by only changing the surface irradiance from the PAR to (PAR plus UVR) based on two MPP models (Vertically Generalized Production Model (VGPM) and Honda–2009 model (Honda et al., 2009); and the equations can be found in Appendix A). The results show that the UVR may increase the annual productivity of phytoplankton by 0.07% (VGPM) and 6.54% (Honda–2009 model) on average. Moreover, in some areas, the increase of the MPP due to the UVR can be up to 6.61% and 75.39% through the use of the VGPM and Honda et al.'s (2009) model, respectively. The large difference between these two models may result from the processing of surface irradiance in the models. In the VGPM, the surface radiation irradiance is processed in the form of $E_0/(E_0+4.1)$ (Eq. (A1)). For the surface PAR ranging from 0 to 300 W/m^2 and UVR ranging from 0 to 40 W/m^2, the difference between the (PAR plus UVR) and the PAR is very small (0.07%). However, in Honda–2009 model, the primary productivity is a linear function of the surface solar irradiance (Eq. (A2)). In this respect, the UVR has a non-negligible effect on the estimation of the MPP. However, it must be noted that the main factor affecting the primary productivity by the VGPM is the max-

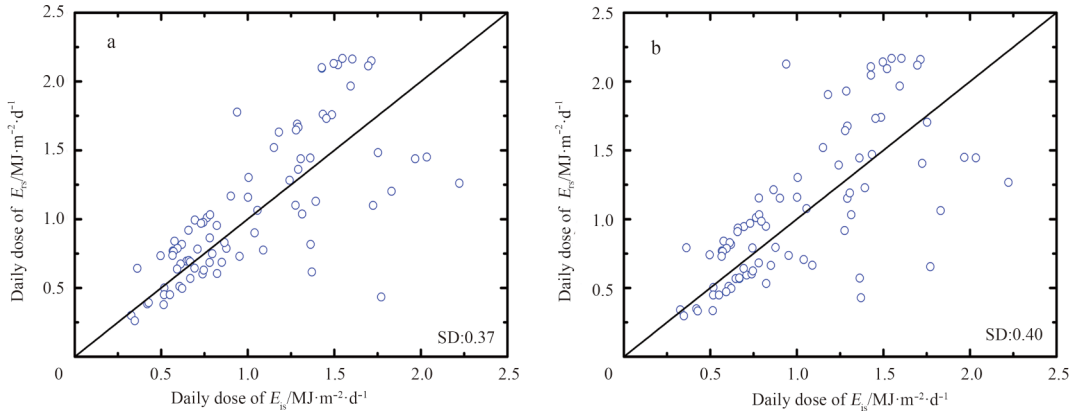

Fig. 7. Comparisons of the daily dose of UV between satellite inversion results (E_{rs}) and *in situ* observations (E_{is}) in 2006. Inversion results from "Terra" and "Aqua" satellite products (a) and inversion products from only the "Aqua" satellite data (b).

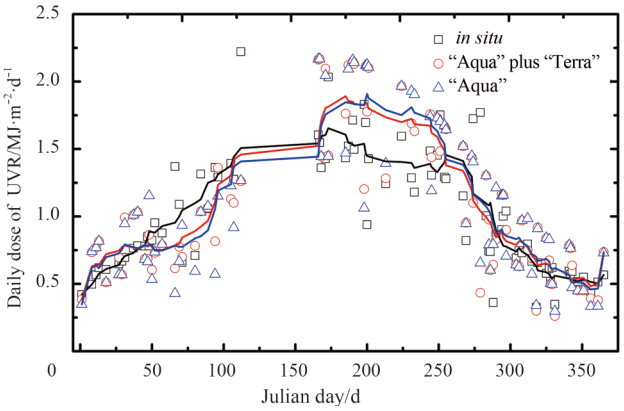

Fig. 8. The annual variation of daily dose of UV in 2006 at San Diego, USA. The symbols are the daily dose, while the lines indicate the 10 d smoothing averaged results, with black, red, and blue indicating the UV irradiance of field observation, UV irradiance retrieved by two-satellite data ("Terra" and "Aqua"), and single "Aqua" data, respectively.

imum carbon fixation rate P^{b}_{opt} (Behrenfeld and Falkowski, 1997), and here we only estimate the MPP by simply changing the UVR-contained irradiance in the MPP model with the unchanged P^{b}_{opt}. Recently, research has shown that the inhibition effects of the UVA and the UVB on the carbon fixation rate of sea surface phytoplankton ranged from –25.00% to 28.90% and 0.34% to 26.50% with an increase in distance offshore (from about 50 to 650 km), respectively (Li et al., 2011). Unlike the 6.54% primary production increment due to the UVR by only changing the surface irradiance, the UVR could improve the annual averaged primary productivity by 2.05% on average under the assumption that the effects of the UVR and the PAR on phytoplankton productivity are the same (Eq. (A3)). Very few models exist for the estimation of carbon fixation rate that consider the effect of the UVR, which retrieve P^{b}_{opt} by using the sea-surface temperature or surface PAR irradiance (Megard, 1972; Ishizaka et al., 2007). Actually, the intensity of UVR, the exposure period of phytoplankton under UVR, and the species composition of the phytoplankton community are the main factors controlling the physiological response of phytoplankton to the UVR (Wu and Gao, 2011; Li et al., 2015). Therefore, more efforts should be made to establish the regional primary productivity algorithm considering the UVR effects. Over a long time scale, the UVR intensity on the sea surface is likely to increase due to the decline of the stratospheric ozone layer (Madronich et al., 1998) or decrease due to the increase of cloud cover (He et al., 2013) and the decrease of the atmospheric concentrations of ozone depleting substances (McKenzie et al., 2011); more satellite products are needed to monitor the long-term effects of the UVR on the MPP on a global scale (Behrenfeld et al., 1993).

References

Agustí S, Llabrés M. 2007. Solar radiation-induced mortality of marine pico-phytoplankton in the oligotrophic ocean. Photochem Photobiol, 83(4): 793–801

Ahmad Z, Herman J R, Vasilkov A P, et al. 2003. Seasonal variation of UV radiation in the ocean under clear and cloudy conditions. In: Optical Science and Technology. SPIE's 48th Annual Meeting. SPIE, International Society for Optics and Photonics, 5156: 63–73

Barbieri E S, Villafañe V E, Helbling E W. 2002. Experimental assessment of UV effects on temperate marine phytoplankton when exposed to variable radiation regimes. Limnol Oceanogr, 47(6): 1648–1655

Behrenfeld M J, Falkowski P G. 1997. Photosynthetic rates derived from satellite-based chlorophyll concentration. Limnol Oceanogr, 42(1): 1–20

Behrenfeld M J, Hardy J T, Gucinski H, et al. 1993. Effects of ultraviolet-B radiation on primary production along latitudinal transects in the South Pacific Ocean. Mar Environ Res, 35(4): 349–363

Campbell J, Antoine D, Armstrong R, et al. 2002. Comparison of algorithms for estimating ocean primary production from surface chlorophyll, temperature, and irradiance. Global Biogeochem Cycles, 16(3): 9–1–9–15

Cullen J J, Davis R F, Huot Y. 2012. Spectral model of depth—integrated water column photosynthesis and its inhibition by ultraviolet radiation. Global Biogeochem Cycles, 26, GB1011: 1–19

Friedrichs M A M, Carr M E, Barber R T, et al. 2009. Assessing the uncertainties of model estimates of primary productivity in the tropical Pacific Ocean. J Mar Syst, 76(1–2): 113–133

Frouin R, Pinker R T. 1995. Estimating photosynthetically active radiation (PAR) at the earth's surface from satellite observations. Remote Sens Environ, 51(1): 98–107

Gao Kunshan, Li Gang, Helbling E W, et al. 2007. Variability of UVR effects on photosynthesis of summer phytoplankton assemblages from a tropical coastal area of the South China Sea. Photochem Photobiol, 83(4): 802–809

Gao Kunshan, Wu Yaping, Li Gang, et al. 2007. Solar UV radiation drives CO2 fixation in marine phytoplankton: a double-edged sword. Plant Physiol, 144(1): 54–59

Guo Shichang, Qin Yu, Zhao Bolin, et al. 2002. The research of the effects of the atmosphere to the ultraviolet radiation. Acta Scientiarum Naturalium Universitatis Pekinensis (in Chinese), 38(3): 334–341

Häder D P. 2011. Does enhanced solar UV-B radiation affect marine primary producers in their natural habitats? Photochem Photobiol, 87(2): 263–266

He X Q, Bai Y, Pan D L, et al. 2013. Satellite views of the seasonal and interannual variability of phytoplankton blooms in the eastern China seas over the past 14 yr (1998–2011). Biogeosciences, 10: 4721–4739

Herman J R, Krotkov N, Celarier E, et al. 1999. Distribution of UV radiation at the earth's surface from TOMS-measured UV-backscattered radiances. J Geophys Res Atmos, 104(D10): 12059–12076

Honda M C, Sasaoka K, Kawakami H, et al. 2009. Application of underwater optical data to estimation of primary productivity. Deep-Sea Research Part I: Oceanographic Research Papers, 56(12): 2281–2292

Hou Xiaowei, Liao Yinghui, Cao Chunli, et al. 2012. Characteristics of the spatial and temporal distribution of solar ultraviolet radiation in Hebei. J Arid Meteorol (in Chinese), 30(4): 583–587

Ishizaka J, Siswanto E, Itoh T, et al. 2007. Verification of vertically generalized production model and estimation of primary production in Sagami Bay, Japan. J Oceanogr, 63(3): 517–524

Jin Zhonghai, Charlock T P, Rutledge K, et al. 2006. Analytical solution of radiative transfer in the coupled atmosphere-ocean system with a rough surface. Appl Opt, 45(28): 7443–7455

Jin Lili, He Qing, Cao Xing. 2009. The summary of research on ultraviolet radiation. Desert Oasis Meteorol (in Chinese), 3(3): 1–6

Jin Zhonghai, Stamnes K. 1994. Radiative transfer in nonuniformly refracting layered media: atmosphere-ocean system. Appl Opt, 33(3): 431–442

Li Gang, Gao Kunshan. 2013. Cell size-dependent effects of solar UV radiation on primary production in coastal waters of the South China Sea. Estuaries and Coasts, 36(4): 728–736

Li Gang, Gao Kunshan, Gao Guang. 2011. Differential impacts of solar UV radiation on photosynthetic carbon fixation from the coastal to offshore surface waters in the South China Sea. Photochem Photobiol, 87(2): 329–334

Li Teng, Bai Yan, Li Gang, et al. 2015. Effects of ultraviolet radiation on marine primary production with reference to satellite remote sensing. Front Earth Sci, 9(2): 237–247

Madronich S, McKenzie R L, Björn L O, et al. 1998. Changes in biologically active ultraviolet radiation reaching the earth's surface. J Photoch Photobio B, 46(1–3): 5–19

McKenzie R L, Aucamp P J, Bais A F, et al. 2011. Ozone depletion and climate change: impacts on UV radiation. Photoch & Photobio Sci, 10(2): 182–198

Megard R O. 1972. Phytoplankton, photosynthesis, and phosphorus in Lake Minnetonka, Minnesota. Limnol Oceanogr, 17(1): 68–87

Nilawati J, Greenberg B M, Smith R E. 1997. Influence of ultraviolet radiation on growth and photosynthesis of two cold ocean diatoms. J Phycol, 33(2): 215–224

Pang Shenghui, Yu Haifeng, He Yunya, et al. 2010. Response of Cyanobacterias to UV radiation. Food Sci Technol (in Chinese), 35(9): 41–45

Smyth T J. 2011. Penetration of UV irradiance into the global ocean. J Geophys Res Oceans, 116(C11): doi: 10.1029/2011JC007183

Tanskanen A, Krotkov N A, Herman J R, et al. 2006. Surface ultraviolet irradiance from OMI. IEEE Trans Geosci Remote Sens, 44(5): 1267–1271

Torres O, Tanskanen A, Veihelmann B, et al. 2007. Aerosols and surface UV products from ozone monitoring instrument observations: An overview. J Geophys Res: Atmospheres (1984–2012),

112(D24): doi: 10.1029/2007JD008809

Vasilkov A, Krotkov N, Herman J, et al. 2001. Global mapping of underwater UV irradiances and DNA-weighted exposures using total ozone mapping spectrometer and sea-viewing wide field-of-view sensor data products. J Geophys Res Oceans, 106(C11): 27205–27219

Wang Pucai, Lu Daren, Li Zhanqing. 2001. A parameterization method for retrieving surface uvb radiation from satellite. Chin J Atmos Sci (in Chinese), 25(1): 1–15

Wang Pucai, Wu Beiying, Zhang Wenxing. 1999. Analysis on the factors affecting surface UV radiation. Chin J Atmos Sci (in Chinese), 23(1): 1–8

Wu Yaping, Gao Kunshan. 2011. Photosynthetic response of surface water phytoplankton assemblages to different wavebands of UV radiation in the South China Sea. Haiyang Xuebao (in Chinese), 33(5): 146–151

Appendix:

A. Marine primary productivity models for the assessment of effects of the ultraviolet radiation

Much research has involved remote sensing models of MPP using the PAR at the visible light (Campbell et al., 2002; Friedrichs et al., 2009). However, to the best of our knowledge, few remote sensing models considering the effects of UVR have never been reported. To evaluate the effects of the UVR on the MPP, two models of the MPP were used by simply changing the surface irradiance with and without the UVR, one is the widely used VGPM (Behrenfeld and Falkowski, 1997) (Eq. (A1)), and the other is the model of Honda et al. (2009) (Eq. (A2) and Eq. (A3)), as follows:

$$MPP = C_{\mathrm{opt}} \times Z_{\mathrm{eu}} \times P^{\mathrm{b}}{}_{\mathrm{opt}} \times D_{\mathrm{irr}} \times \left[0.661\,2 \times E_0/\left(E_0 + 4.1\right)\right], \quad \text{(A1)}$$

$$MPP = C_{\mathrm{int}} \times E_0 \times \Psi, \quad \text{(A2)}$$

$$\Psi = 3.41(E_0)^{-0.68}, \quad \text{(A3)}$$

where $P^{\mathrm{b}}{}_{\mathrm{opt}}$ is the maximum carbon fixation rate of phytoplankton in the euphotic layer (mg C/((mg Chl-*a*)·h)); C_{opt} is the chlorophyll *a* (Chl-*a*) concentration at the depth of $P^{\mathrm{b}}{}_{\mathrm{opt}}$ ((mg Chl-*a*)/m^3); Z_{eu} is the depth of the euphotic layer; D_{irr} is the sunshine period (day length); E_0 is the daily photosynthetically active radiation at the sea surface (Einstein/(m^2·d)); C_{int} is the integrated concentration of chlorophyll *a* in the euphotic layer (mg/m^2); and Ψ is the utilization efficiency of solar radiation by phytoplankton (mg C/((mg Chl-*a*)·(mol quanta))).